

CRYSTALLITE THICKNESS AND DEFECT DENSITY OF PHYLLOSILICATES IN LOW-TEMPERATURE METAMORPHIC PELITES: A TEM AND XRD STUDY OF CLAY-MINERAL CRYSTALLINITY-INDEX STANDARDS

LAURENCE N. WARR¹

Geologisch-Paläontologisches Institut, Ruprecht-Karls-Universität, Im Neuenheimer Feld 234, 69120 Heidelberg, Germany

FERNANDO NIETO¹

*Departamento Mineralogía y Petrología, Instituto Andaluz de Ciencias de la Tierra,
Universidad de Granada – Consejo Superior de Investigaciones Científicas, E-18071 Granada, Spain*

ABSTRACT

The thickness distribution and defect density of illite crystallites (both illite–smectite and illite–muscovite phases) and chlorite are presented for a set of clay-mineral crystallinity-index standards, as determined by TEM and XRD methods for both the whole rock and disaggregated clay-sized fractions. The pelitic standards, selected from the Variscan rocks of southwestern England, display the full array of typical microstructural transformations that characterize the prograde transition from diagenesis (zeolite facies) to epizone (greenschist facies), with increasing thickness of crystallites and decreasing concentration of lattice imperfections. Crystallite thickness, measured from TEM lattice-fringe images in the c^* direction of both illite and chlorite, commonly deviate from lognormal distributions, with positive skewness toward small sizes. These distributions are considered to reflect complex histories of nucleation and growth, as well as structural modifications due to rock strain. Crystal damage caused by rock disaggregation, in the form of splitting along crystallite boundaries and other planar defects, can be observed in all clay-sized separates. The degree of damage increases as a function of increasing size of crystals, and clearly enhances the differences in mean thickness of the crystallites between the whole rock and clay-sized fractions, particularly in anchizonal and epizonal slates. Although clay separates yield smaller mean thicknesses of crystallites and show thickness distributions with lower degrees of skewness and standard deviation than measured from matrix of the pelitic rocks, the α and β_2 shape parameters (the mean and variance of the natural logarithms of the sizes) for both grain-size fractions define a common crystal-growth path when plotted in $\alpha - \beta_2$ space. This feature shows that ultrasonic disaggregation has not modified the shape of the thickness distributions in a way that has influenced the interpretation of the mechanisms of crystal growth and deformation. NEWMOD modeling of XRD profiles based on TEM constraints show a relatively good correspondence between the size of X-ray-scattering domains and crystallite thicknesses in most cases. XRD-determined area-weighted mean thicknesses of crystallites calculated using an integral peak-width method yield sizes that correspond to those measured directly from TEM measurements. However, the refined Warren–Averbach method of MUDMASTER, adopted for the analysis of PVP-saturated clays, produced profiles that do not match well the TEM-determined distributions. Refinements to the method are required before accurate thickness-distributions can be extracted from the narrower XRD reflections of metamorphic phyllosilicates.

Keywords: phyllosilicates, clay minerals, crystallite thickness, defect density, transmission electron microscopy, X-ray diffraction, crystallinity-index standards, low-temperature metamorphism, pelites.

SOMMAIRE

Nous documentons la distribution de l'épaisseur et la densité de défauts des cristallites d'illite (soit illite–smectite ou illite–muscovite) et de chlorite dans une collection d'étalons d'argile servant à l'évaluation de leur cristallinité, telle que déterminée en microscopie électronique par transmission (TEM) et par diffraction X d'échantillons de roches totales et de fractions d'argile désagrégée. Les étalons de pélites, choisis parmi les roches varisques du sud-ouest de l'Angleterre, montrent le spectre complet de transformations microstructurales typiques de la transition prograde à partir de la diagenèse (faciès zéolite) à l'épizone (faciès schistes-verts), par exemple l'augmentation de l'épaisseur des cristallites et la diminution de la proportion de défauts dans le réseau. L'épaisseur des cristallites, mesurée à partir d'images de franges réticulaires de l'illite et de la chlorite dans la direction c^* , s'écarte généralement d'une distribution log-normale, avec un décalage en faveur des tailles plus petites. Ces distributions résulteraient d'une séquence complexe d'événements de nucléation et de croissance, aussi bien que de modifications structurales dues à la déformation des roches. Le dommage dû à la désagrégation des échantillons de roche, par exemple la séparation le long

¹ E-mail addresses: hq0@ix.urz.uni-heidelberg.de, fnieto@goliat.ugr.es

d'interfaces entre cristallites et autres défauts planaires, se voit dans chaque concentré de particules d'argiles. Le degré d'endommagement augmente avec la taille des cristaux, et exagère évidemment la différence en épaisseur moyenne des cristallites entre la roche totale et les concentrés d'argile, en particulier dans le cas d'ardoises de l'anchizone et de l'épizone. Quoique les concentrés d'argile possèdent des cristallites plus minces qui font preuve d'une distribution d'épaisseurs avec moins d'asymétrie et un écart-type moins important que ceux qui caractérisent la matrice de roches pélitiques, les paramètres α et β_2 décrivant la forme des particules (la moyenne et la variance des logarithmes naturels des dimensions) pour les deux fractions granulométriques définissent un tracé commun de croissance cristalline. Cette observation montre que la désagrégation ultrasonique n'a pas modifié la distribution des épaisseurs de cristallites d'une façon qui a influencé l'interprétation des mécanismes de croissance cristalline et de déformation. La simulation des profils de diffraction X avec le logiciel NEWMOD et les contraintes apportées par les observations TEM montrent une correspondance assez bonne entre la taille des domaines responsables de la dispersion des rayons X et l'épaisseur des cristallites dans la plupart des cas. L'épaisseur des cristallites déterminée par diffraction X selon la largeur des pics et corrigée pour l'aire des particules correspond à celle qui est mesurée directement par TEM. Toutefois, l'affinement par la méthode de Warren–Averbach du logiciel MUDMASTER, adopté pour l'analyse des argiles saturées en PVP, donne des profils qui ne concordent pas bien avec les distributions mesurées en TEM. De nouveaux affinements de la méthode seront nécessaires avant que l'évaluation de la distribution d'épaisseurs puisse venir des réflexions plus étroites des spectres de diffraction des phyllosilicates métamorphiques.

(Traduit par la Rédaction)

Mots-clés: phyllosilicates, argiles, épaisseur des cristallites, densité des défauts, microscopie électronique en transmission, diffraction X, étalons de cristallinité, métamorphisme de basse température, pélites.

INTRODUCTION

Phyllosilicate crystals that grow at low temperatures are characteristically small and rich in defects. Significant changes in the size of small crystals (\approx crystallites), and in the type and concentration of their lattice imperfections, such as lattice distortion, dislocations and planar defects, including stacking faults and polysomatic structures, occur in response to varying physicochemical environment within both diagenetic and metamorphic rocks (Lee *et al.* 1985, Ahn & Peacor 1986, 1989, Banfield *et al.* 1994, Dalla Torre *et al.* 1996). Recognition and quantification of these microstructures can provide information concerning processes of growth and mechanisms of deformation accompanying crystallization and recrystallization (Cashman & Ferry 1988, Eberl *et al.* 1990, 1998a, Merriman *et al.* 1995). Such documentation also is important in assessing the physical and chemical properties of phyllosilicates for industrial applications.

Two principal approaches are available to study the microstructure of phyllosilicates: direct imaging using high-resolution transmission electron microscopy (TEM), and indirect determination through the analysis of electron diffraction and X-ray diffraction (XRD) scattering effects. During the last 10–15 years, these methods have been extensively applied to the study of low-temperature phyllosilicates in both diagenetic and metamorphic rocks. Particular attention has been given to the nature of diagenetic mixed-layered illite–smectite (Ahn & Peacor 1986, 1989, Veblen *et al.* 1990, Środoń *et al.* 1990, Środoń & Elsass 1994), and to the microstructural changes that accompany its prograde metamorphic transition to illite–muscovite within the mudstone-to-slate transition (Merriman *et al.* 1990,

1995, Árkai *et al.* 1996, Jiang *et al.* 1997, Dalla Torre *et al.* 1996, Livi *et al.* 1997). Typical prograde changes in illite (a general term encompassing both illite–smectite and illite–muscovite phases) involve an increase in authigenic phases at the expense of detrital minerals, an increase in crystallite size, a decrease in the amount of swelling layers (interlayered smectite), the transition from poorly ordered diagenetic $1M_d$ to well-ordered metamorphic $2M$ polytypes, and a general decrease in the concentration of lattice imperfections. Particularly important are the changes in crystallite-size distributions of authigenic and metamorphic phases, which can yield information concerning the original conditions of nucleation, the growth mechanisms involved (Eberl *et al.* 1990, 1998a) and modifications due to deformation or annealing (Cashman & Ferry 1988, Merriman *et al.* 1995).

In this study, we investigate the microstructure of phyllosilicates by detailed TEM and XRD analysis of a set of four internationally available samples of pelitic rock, which span a prograde mudstone-to-slate transition in the Variscides of southwestern England. Data on crystallite thickness and defect density in illite and chlorite, measured from high-resolution TEM lattice-fringe images of both whole-rock and clay-sized fractions, are presented. These constraints are used to consider the mechanisms of crystal growth and deformation, to assess the damage incurred by disaggregation of the clay fractions prepared for XRD analysis, to evaluate which microstructural features observed in TEM images act as X-ray scattering domains by modeling using the NEWMOD program of Reynolds (1985), and finally, to test some recently refined methods for improved measurement of mean thickness and thickness distributions of crystallites by the XRD approach.

REVIEW OF THE XRD APPROACH

The most commonly applied technique for the general characterization of prograde microstructural transformations is the XRD-based index of clay-mineral crystallinity, measured by the FWHM (full width at half maximum) of a prominent basal reflection of a phyllosilicate. Illite crystallinity (IC) records changes in very low metamorphic grade through the progressive sharpening of the 10 Å basal reflection of illite (the Kübler index); although mostly influenced by the thickness of crystallites (Merriman *et al.* 1990), it also may be affected by interlayers of smectite (Nieto & Sánchez-Navas 1994) and, to a minor degree, by lattice distortion (Árkai *et al.* 1996). The IC method therefore constitutes a general measure of the microstructural and mineralogical transformations that occur during the transition from illite–smectite to illite–muscovite during prograde metamorphism (Peacor 1992, Jiang *et al.* 1997). Similar mechanisms are also envisaged for the changes underlying chlorite crystallinity (Árkai *et al.* 1996, Merriman *et al.* 1995).

As a result of the number of crystal-chemical parameters that may influence clay-mineral crystallinity, a principal challenge is to find procedures that can resolve individual crystallographic features from broadened XRD profiles and, in particular, extract thickness distributions of crystallites. Two advances have recently been presented which claim to enable such information to be obtained from diffraction profiles of clay minerals. The first is the software package MUDMASTER (Eberl *et al.* 1996), which applies a modified Warren–Averbach (W–A) method to extract information about crystallite thickness and lattice distortion (strain) from asymmetrically broadened XRD profiles of clay minerals. The second is a sample-preparation technique for illite–smectite that uses polyvinylpyrrolidone (PVP), which provides highly oriented homogeneous films of clay without swelling (Eberl *et al.* 1998b). The application of Fourier-based methods on phyllosilicates in low-temperature metamorphic pelites, which commonly contain crystallite thicknesses in excess of 20 nm, has been brought into question (Lanson & Kübler 1994, Árkai *et al.* 1996, Warr 1996), as commercially available software yielded crystallite thicknesses judged to be too small and of unsatisfactory precision.

Despite advances in the XRD approach, a number of analytical problems may inhibit the routine and effective measurement of geologically meaningful phyllosilicate microstructure. The first problem, highlighted by Jiang *et al.* (1997) and the subject of a study by Li *et al.* (1998), concerns the microstructural damage incurred by phyllosilicates during disaggregation of the clay-size fraction. This effect is of particular concern in the case of rocks, where damage will invariably occur during breakage of interlocking minerals. As the grinding of minerals is known to modify the shapes and size distributions of crystals, it is critical to understand

the nature of these modifications before effective interpretations can be drawn concerning mineral processes in nature. A second problem concerns the notorious sensitivity of XRD results to differences in the analytical conditions adopted. As crystallinity measurements are empirical in nature, interlaboratory differences in analytical data may be standardized by calibration to an accepted scale of measurement using sets of internationally available standards. Such an approach was presented by Warr & Rice (1994), and a standard scale, referred to as the Crystallinity Index Standard (CIS), was defined. In the case of crystallite thicknesses (measured by sizes of X-ray scattering domains), the standardization of data is not straightforward, because theoretically derived crystallite thickness is a quantifiable measure for which correct values exist. Although empirical data on crystallite thickness were introduced in the context of the CIS by Warr & Rice (1994), based on Scherrer and W–A methods of profile analysis, there is an obvious advantage if the accuracy of such values can be verified by TEM.

CRYSTALLINITY-INDEX STANDARDS

The crystallinity-index standards analyzed in this study consist of four pelitic rocks from the Variscan low-temperature metamorphic belt of north Cornwall, southwestern England, which range from diagenetic (zeolite facies) to epizonal (greenschist facies) grades. Some details concerning mineralogy and fabric description are outlined as follows.

Standard SW1 is a silty late diagenetic mudstone (IC = $0.63^\circ\Delta 2\theta$) with a $<2\ \mu\text{m}$ fraction of illite–smectite, chlorite, quartz and albite. Minor amounts of kaolinite were detected in both whole-rock and clay-mineral fractions (previously not recognized). The mudstone is homogeneous, with a blocky fracture, but lacks a penetrative tectonic cleavage. Microscopically, a strong bedding-parallel fabric is seen by the preferred orientation of grains of detrital mica. The grain size of detrital mica and subangular quartz is commonly 10–20 μm , but the matrix is generally much finer ($<2\ \mu\text{m}$).

Standard SW2 is a cleaved silty mudstone of diagenetic grade (IC = 0.47, kaolinite crystallinity = $0.30^\circ\Delta 2\theta$), collected close to a regionally mapped boundary of the anchizone (Warr *et al.* 1991). The rock consists mostly of quartz, illite, kaolinite (presumably dickite) and plagioclase, with minor amounts of K-feldspar, detrital opaque minerals and secondary carbonate. The $<2\ \mu\text{m}$ fraction is characterized by illite–smectite, kaolinite, some discrete grains of smectite, and an absence of chlorite. At the microscopic level, grains of detrital mica up to 20–30 μm long are visible, as well as abundant subangular grains of quartz. A bedding-parallel fabric, marked by the orientation of mica grains, is overprinted by a spaced anastomosing pressure-solution cleavage. Some grains of detrital mica have been rotated parallel to the tectonic fabric.

Standard SW4 is an anchizonal grey slate [IC = 0.38, chlorite crystallinity (ChC) = $0.32^\circ\Delta 2\theta$] of the prehnite–pumpellyite facies, which has a well-developed slaty cleavage. The sample contains pre- or synkinematic stacks of chlorite–mica similar to those described by Warr *et al.* (1991), and a discrete synkinematic phase of mica growth is observed within surrounding strain shadows. The slaty fabric is overprinted by a weak crenulation cleavage. The whole-rock assemblage in SW4 consists of illite–muscovite, chlorite, quartz, and feldspar (K-feldspar and albite). The main minerals in the $<2\ \mu\text{m}$ fraction are illite–muscovite with minor paragonite, chlorite, quartz, and feldspar.

Standard SW6 is a green-grey epizonal slate (IC = 0.25, ChC = $0.25^\circ\Delta 2\theta$) of the greenschist facies. The mineralogy of SW6 consists of mostly illite–muscovite, ferroan chlorite, quartz, with minor albite and ilmenite. The sample contains a good slaty cleavage, across which postkinematic porphyroblasts of muscovite have grown. The $<2\ \mu\text{m}$ fraction of SW6 consists of $2M_1$ illite–muscovite, chlorite, with traces of quartz, albite and discrete particles of smectite as an alteration product.

The *muscovite instrumental standard MF1* is a flake (parallel to 001) 60–80 μm thick from a euhedral crystal of muscovite, obtained from a granite pegmatite in India.

ANALYTICAL METHODS

Transmission electron microscopy

Standard material was selected at random from the collection of clay mineral crystallinity-index standards at the University of Heidelberg. From this material, sticky-wax thin sections were prepared, oriented perpendicular to the main rock fabric of each sample. Thin sections were investigated optically and by back-scatter scanning electron microscopy to select homogeneous areas for further study. Several 3-mm copper rings with a hole 1 mm in diameter were glued to areas of fine matrix using a low-vapor-pressure epoxy resin. After adhesion, the rings were again optically examined in order to select matrix-rich preparations lacking large detrital grains or porphyroblasts. After drying for 24 hours, the rings were removed by heating with a soldering iron from the reverse side of the thin section. The preparations were then finally washed in acetone to remove any resin from the sample surface, and then ion-thinned to a suitable thickness for TEM study.

Clay fractions ($<2\ \mu\text{m}$) were separated from the sample rock material following the exact procedure described by Warr & Rice (1994). The disaggregation method was that of gentle ultrasonic treatment in a bath for up to 2–3 hours. The clay-in-suspension was strongly diluted, thoroughly mixed, and pipetted into Agar rubber mounds. The solution dried in approximately 12 hours, producing thin sedimented preparations. When completely dry, the samples were soaked in ethanol for

15 minutes, and then impregnated using a Spurr resin kit. Ultrathin sections were then cut perpendicular to the sedimented clay film using a diamond knife.

TEM work was undertaken at the University of Granada, using a CM20 Philips STEM microscope at an operating voltage of 200 kV. High-resolution images were obtained at a range of magnifications between 50,000 and 350,000. Measurements were made either using a projecting microscope with a magnification of $18\times$, or by direct measurement on $30 \times 40\ \text{cm}$ photographic prints. This study presents the results based on a total of 413 lattice-fringe image negatives, 85 selected-area electron-diffraction (SAED) patterns, and was supported by energy-dispersion analyses (scanning TEM mode) of selected sites of interest.

Microstructural measurements from TEM lattice fringe images

A schematic presentation of the microstructural features commonly observed in phyllosilicates is presented in Figure 1. A vertical stack of five crystallites of illite (thicknesses of 5, 15, 5, 5, 5 nm, respectively) and a single intervening crystallite of chlorite (thickness 7 nm) are shown in the form of a block projection. The crystallites contain defects such as layer terminations, layer-parallel planar faults with incoherent rotations of layers, high-strain fields, dislocation lines within 001, and collapsed swelling layers.

Crystallites represent a succession of optically parallel and uninterrupted layers of equivalent d -value in the plane perpendicular to 001 (crystallographic direction c^*). Crystallite thickness (T_L) is measured as the distance between obvious angular discontinuities in the orientation of these layers, or by a systematic change in the mineral's d -value (*e.g.*, the illite–chlorite boundaries in Fig. 1). High-angle crystallite boundaries ($>5^\circ$) are readily resolvable in TEM images, whereas low-angle crystallite boundaries are more difficult to distinguish and can be less reliably determined. In section A of the block diagram, a low-angle boundary can be observed between the second and third crystallite from the bottom of the stack. However, the same boundary is parallel in section B, and counted as an intracrystalline defect.

In addition to T_L , a defect-free distance (T_δ) was measured as the interval between intracrystalline defects that do not have recognizable angular discontinuities between layers in the c^* direction. Defects may comprise layer terminations, layer-parallel planar defects with incoherent rotations of layers, dislocation lines (emphasized by layer partings due to beam damage), and collapsed swelling layers. Such defects were commonly recognized by distinct variations in contrast across layers caused by local variations in lattice orientation, causing strain fields. As the exact nature of each defect could not always be recognized on a routine basis, it is likely that a certain proportion of the planar defects measured

are stacking faults, or layer partings that may have arisen from ion-milling or electron-beam damage. T_8 therefore represents a general approximation of defect density, rather than a specific measure of the defects that cause broadening of XRD 001 reflections.

As T_L and T_8 commonly vary within the (001) plane, multiple measurements (usually 600–1600 counts per preparation) were recorded at ~100 nm intervals along the lengths of grains. From these data, the mean thickness of crystallites was then calculated for between 45 to 633 crystallites per preparation. The length of crystallites was also estimated from TEM images. In the whole-rock samples, these lengths represent minimum values because the crystallites are commonly longer than the image, or only one end of the crystallite is in the field of view. Although in ultramicrotomed clay separates both ends of crystallites could commonly be observed, these are also considered to represent minimum values because of recognizable breakage of particles along their lengths incurred during cutting with the diamond knife.

N-weighted \bar{T}_L and \bar{T}_8 data, and thickness distributions, were plotted directly from the TEM measurements. Area- and volume-weighted mean thicknesses were approximated using the thickness and length measurements of the crystallites by assuming that the grains are flat square-shaped plates with sides of equal length (as shown in Fig. 1). Distributions of area-weighted thickness for the clay-sized fractions were also estimated for direct comparison with thicknesses measured by XRD methods. Investigation of the basal surfaces of the dispersed clay fraction by TEM showed grain shapes to vary considerably in all samples. The most commonly observed shape of a phyllosilicate is rectangular, with occasional pseudo-hexagonal outlines. Although Jiang *et al.* (1997) assumed hexagonal grain-shapes for weighting mean thicknesses of crystallites from TEM images, such differences in assumed shape are considered to have a minimal effect on sizes calculated in relation to the approximations involved in the measurement of crystallite lengths.

Powder X-ray diffraction

Equal concentrations of <2 μm Na-saturated clay-in-suspension (2.5 mg per 1 mL H_2O) were prepared and stored in capped glass bottles. For measurement, the samples were mixed with polyvinylpyrrolidone with a molecular mass of 10,000 (PVP-10) and sedimented as thin clay films (2.5 mg of clay to 5 mg PVP) onto a silicon wafer substrate (Eberl *et al.* 1998b). All samples were scanned from 4 to $20^\circ 2\theta$ using a Siemens D500 diffractometer. In an attempt to reduce instrumental broadening to a minimum, 1° soller slits and a narrow receiving slit of 0.018° were installed. The dramatic loss of peak intensity incurred using this slit combination was compensated by the use of long count-times, 50 seconds per 0.01° interval. The instrumental standard,

Mf1, was prepared by cutting several flakes into mm-sized fragments using a set of sharp scissors. The fragments were soaked in water for 24 hours and then ultrasonically treated for 10 hours using an ultrasonic bath. The 2–6 μm fraction was separated by centrifugation and then prepared as the previous clay fractions, using Na-saturation and PVP-10 treatment. Mean thicknesses of crystallites (X-ray scattering domains) were calculated by using the integral peak-width method of Drits *et al.* (1998), a Siemens Fourier single-line method (Siemens WINCRYSIZE, version 2.2, 1991), and the W-A method of MUDMASTER (Eberl *et al.* 1996). The latter method was also used to measure the distribution of crystallite thicknesses for the clay separates.

RESULTS

TEM observations of ion-milled whole rock

The matrix of *diagenetic* pelite SW1 is dominated by thin crystallites of illite, which display a variety of fabric relationships. Two generations of illite can be seen in Figure 2A, an older one of pre- or syncompactional origin, which is deflected around a grain of detrital quartz (with associated void spaces), and a younger postcompactional late diagenetic illite, comprising planar and subparallel packets, showing no corresponding deflections. The late diagenetic illite, presented in Figure 2B, comprises thin packets containing low-angle boundaries between crystallites, numerous layer-terminations, and collapsed swelling-layers (10–12 Å layer thicknesses) marked by high contrast and irregular lattice-fringes. T_L and T_8 boundaries are emphasized by local variations in contrast, representing slight changes in orientation. Illite comprises a mixture of $1M_d$ and poorly ordered $2M$ polytypes, which show streaking of non-001 reflections in SAED patterns. The matrix of SW1 also contains subordinate crystallites of chlorite that are stacked, along with illite, into aggregates (quasicrystals of Środoń *et al.* 1990). The boundaries between these aggregates are usually of high-angle type, and may reach 90° . High-angle boundaries are also observed between fine-grained phyllosilicates in the matrix, and occasional large crystallites of both detrital chlorite and illite–muscovite.

In the matrix of pelite SW2, typical of the *diagenesis* – *anchizone* boundary, illite crystallites (mostly of poorly ordered $2M$ polytype) show fewer small-scale variations in orientation, and are arranged in thin continuous straight packets. Figure 3 shows a number of intersecting subparallel packets, with low- and high-angle grain boundaries, which intersect a grain of detrital quartz partially dissolved by pressure solution. The packets are clearly of postcompactional late diagenetic – early metamorphic origin, and show a lower proportion of layer terminations and collapsed swelling-layers (2% measured by XRD) as observed in SW1. Thicker crystallites of illite–muscovite with layer spacings of

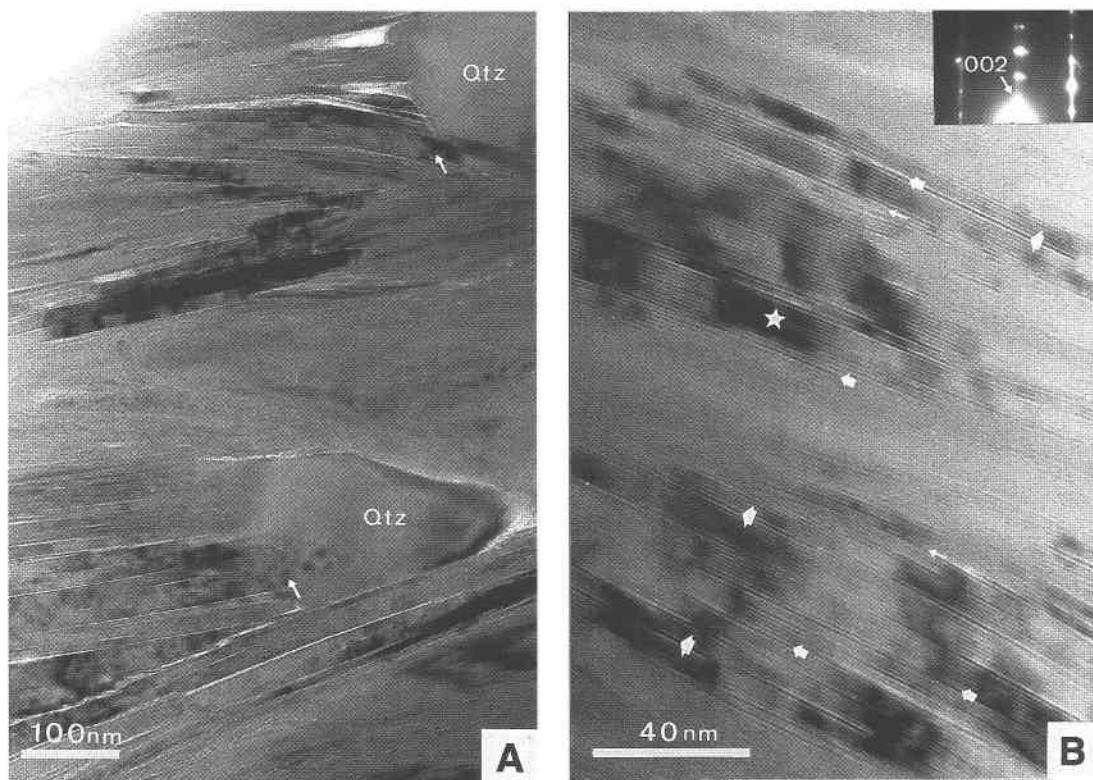


FIG. 2. A) Lattice-fringe image of thin packets of illite from ion-milled diagenetic mudstone SW1. The upper arrow marks a pre- or syncompactional generation of illite, which is deflected around a detrital quartz grain. The lower arrow shows a postcompaction phase of authigenic growth of illite. B) Lattice-fringe image of thin packets of illite showing crystalline boundaries (thin arrows), layer terminations (long fat arrows) and collapsed swelling-layers (short fat arrows). The stars mark areas of high-strain fields (lattice distortion) within the thin heterogeneous packets.

20 Å (well-ordered $2M$ polytype) of likely detrital origin are stacked subparallel to the matrix illite.

The pelitic sample SW4, representative of the *anchizone*, contains significantly thicker and less curved mottled packets of intergrown illite and chlorite (Fig. 4). Larger illite–muscovite packets of well-ordered $2M$ polytype enclose stacks of smaller, more poorly ordered crystallites. These smaller packets are occasionally found to have coalesced into larger crystallites containing fewer defects, which probably reflect annealing and recrystallization fabrics, as described by Merriman *et al.* (1995). Grain boundaries between some illite packets are marked by fringes of high contrast and variable thickness; these fringes probably represent collapsed swelling-layers.

The *epizone* pelite SW6 consists of thick crystallites of illite–muscovite ($2M$ polytype) and chlorite arranged in well-oriented parallel to subparallel packets (Fig. 5A). Illite–muscovite crystallites occur in a range of sizes and defect concentrations, with coalescence of packets simi-

lar to those described in SW4. Cutting across the matrix, large and abundant porphyroblasts of illite–muscovite and, less commonly, chlorite, give rise to a variety of angular relationships between grain boundaries. At the end of crystals, grain boundaries lying 90° to the main foliation can commonly be observed, suggesting that textural equilibrium was attained during growth. A common feature, observed in Figure 5A, is the replacement of defect-rich areas of chlorite by relative defect-free muscovite. This reaction is consistent with the textures observed with the optical microscope, where postkinematic porphyroblasts of muscovite have partly replaced the main slaty fabric. SAED patterns of the chlorite (Fig. 5B) are characteristic of semirandom ordering, with streaking of rows with $k \neq 3n$, similar to those documented by Bons & Schryvers (1989). Fields of high strain (lattice distortion) are common in the vicinity of defects and are usually concentrated along crystallite boundaries. Other common features of matrix chlorite are long-range ordering of the structure and



FIG. 3. Lattice-fringe image of thin crystallites of illite in the ion-milled diagenetic (near anchizonal) mudstone SW2. The upper inset SAED pattern shows a $2M$ polytype of illite of authigenic origin, with a poor degree of ordering in non- $00l$ reflections. The lower inset SAED pattern pertains to a grain of the well-ordered $2M$ polytype of illite, of possible detrital origin, the position of which is marked by an arrow.

polygonization, resembling the deformation-induced microstructures in chlorite described by Bons (1988).

Ultramicrotomed clay-sized fraction

Examples of microstructural features observed in ultramicrotomed clay-sized fractions are shown in Figures 6A–D. General differences in the nature of the clay separates can be seen between the two diagenetic samples and the anchizonal and epizonal separates. In Figures 6A and B, separated grains from diagenetic pelites SW1 and SW2 consist of aggregates in which segments of original fabric are preserved. Figure 6A contains a detrital clast surrounded by small flakes of matrix illite, similar to that observed in the original rock fabric in Figure 2A. A distinct crystallite of illite has wrapped around the clast at a high angle to the main fabric; it presumably belongs to a pre- or syncompaction phase

of growth. Subparallel aggregates of illite crystallites are also observed in Figure 6B. At the top of the main aggregate, a thicker crystallite of illite shows a naturally tapered end, which forms the boundary of the separate. In contrast, the clay fractions of anchizonal and epizonal samples (Figs. 6C, D) contain few remnants of the original fabric; they consist more commonly of individual fragments of partly broken crystals rather than of grain aggregates.

Two causes of damage to crystals are distinguished in the ultramicrotomed clay fractions. The most obvious was caused by microtoming of the clay film with the diamond knife, which fragmented grains into several pieces, particularly along their long axes in the vicinity of air bubbles. It is also conceivable that similar damage occurred within the epoxy resin due to the strong contrast in ductility between resin and clay. Cutting damage was most evident in the two higher-grade metamorphic samples (SW4 and SW6), and less common in the diagenetic samples (SW1 and SW2). Figure 6B shows splitting damage of a grain of diagenetic illite upon entry into an air bubble, whereas a more common type of damage during microtoming is that seen in a defect-rich grain of chlorite from the epizone in Figure 6D, where splitting occurred perpendicular to the long axis (along c^*). Although this type of damage does not strongly modify T_L or T_S measurements, it does affect crystallite length, and therefore presumably influences the area- and volume-weighted T_L sizes calculated from the TEM measurements. The second noticeable form of damage was incurred before cutting and can be attributed to sample disaggregation either during initial crushing or by ultrasonic treatment. Fragmentation of this type can be seen in resin-impregnated areas, and can be distinguished from cutting-induced damage, as no matchable fragments occur adjacent to the point of breakage. Broken edges are commonly irregular, with splitting along natural boundaries of the crystallite as well as along intracrystalline defects. Examples of this type of damage are observed in all fractions (Figs. 6A–D). Occasionally, thinner crystallites show signs of kinking (Fig. 6C), which is also considered to be a result of disaggregation. On the positive side, the broken edges of grains aided recognition of defects within the crystal structure, as these planes of weakness give rise to a step-like edge geometry running roughly perpendicular to 001.

Thickness measurements from TEM images

The results of crystallite thickness and defect-free distance measurements (T_L and T_S) for illite and chlorite in whole-rock and clay-sized fractions are presented in Table 1. A clear increase in N-weighted T_L occurs with increasing metamorphic grade for both phyllosilicates in both fractions. The only exception to this trend is with the thick crystallites of chlorite ($T_L = 53$ nm) in whole-rock diagenetic pelite SW1, which is attributed to a high

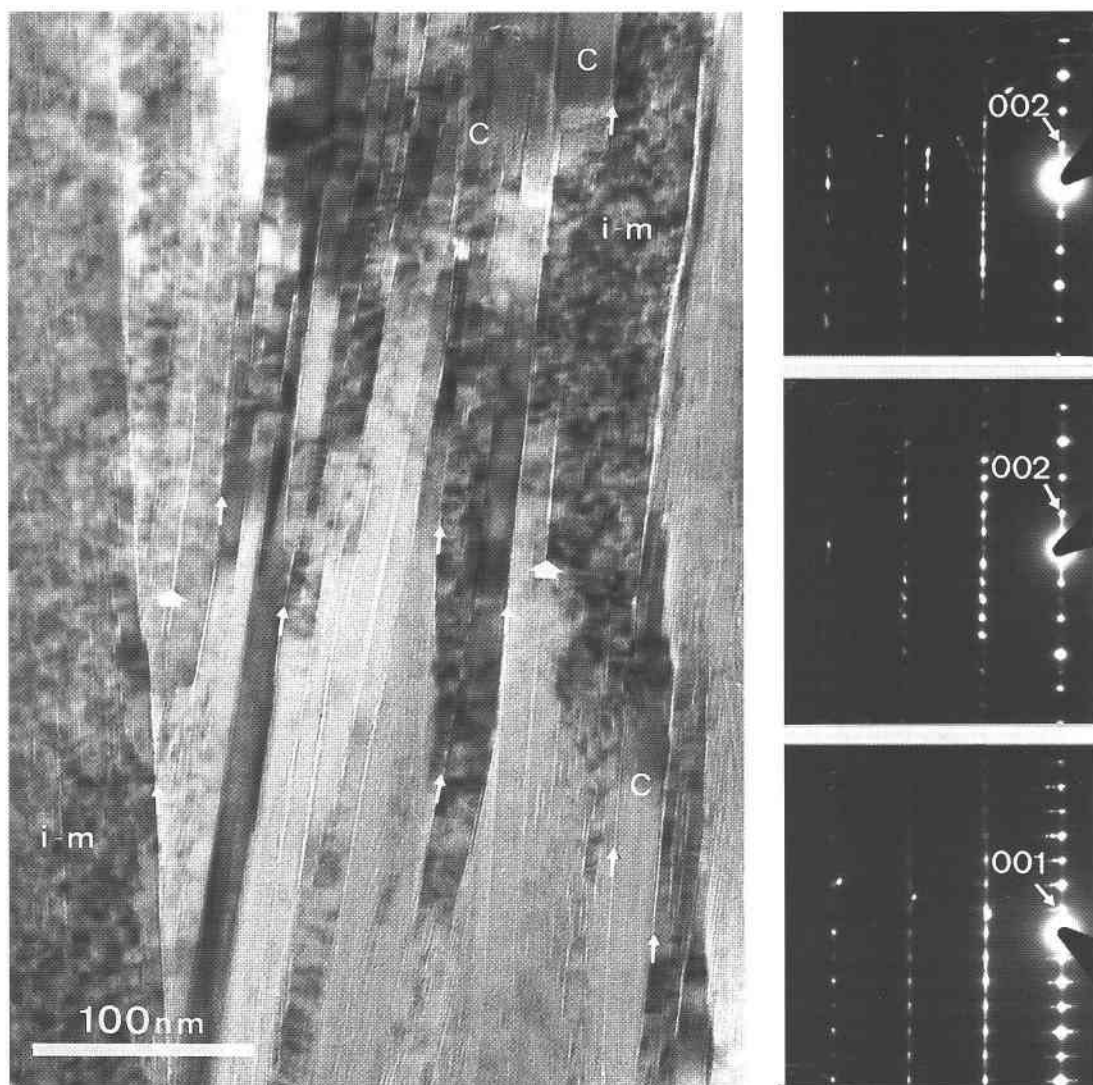


FIG. 4. Lattice-fringe image of illite-muscovite (i-m) and chlorite (c) crystallites in ion-milled anchizonal slate SW4. SAED patterns of illite (top and middle right) are of the $2M$ polytype and show varying degrees of order in non- $00l$ reflections. Chlorite polytypes (bottom right) also show semirandom degrees of order in non- $00l$ reflections. Examples of crystallite boundaries are marked by long thin arrows. Short fat arrows mark the positions of some possible collapsed swelling-layers.

content of the detrital fraction. Although no clear trend exists in \bar{T}_8 thicknesses of the pelites, the epizonal standard SW6 has the lowest concentration of defects, and the diagenetic SW1 is the most defect-ridden. The range of \bar{T}_8 variation within the anchizonal and diagenetic-grade pelites is generally low (11–16 nm).

The two diagenetic-grade pelites show no major difference in \bar{T}_L or \bar{T}_8 values for illite between the whole-rock and clay-sized fractions (Table 1). Distributions of \bar{T}_L in both diagenetic whole-rock fractions are strongly

positively skewed and show large standard deviations from the mean. This large range in size is probably due to a heterogeneous mixture of numerous small crystals of authigenic illite and larger detrital phases, which could not be systematically separated during TEM measurements. Values of \bar{T}_8 in the whole rock of both diagenetic samples also show relatively large variations, with high degrees of skewness and standard deviation values, but they are not as extreme as in \bar{T}_L . In contrast, \bar{T}_L distributions of the diagenetic clay-sized fractions

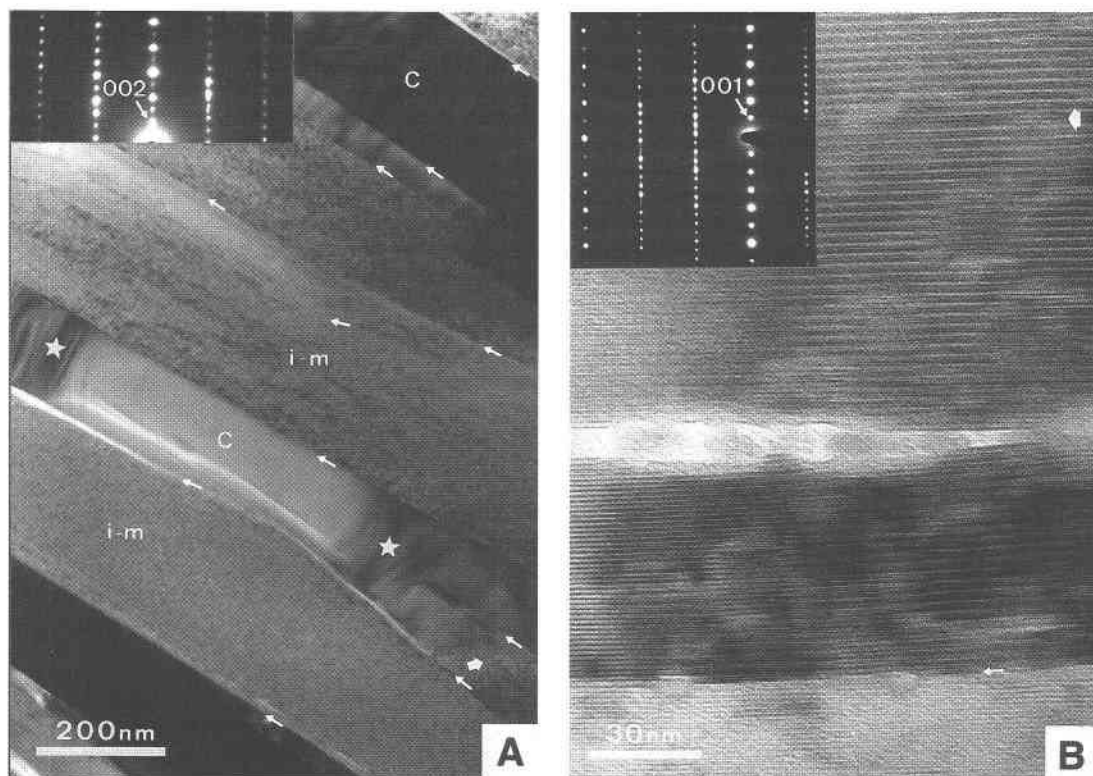


FIG. 5. A) Lattice-fringe image of large crystallites of illite-muscovite and chlorite in ion-milled epizonal slate SW6. The SAED pattern (upper left) shows the well-ordered $2M$ polytype of illite-muscovite, which is seen replacing defect-ridden chlorite (broad arrow in bottom right). The stars mark positions of high-strain fields (lattice distortion). Long narrow arrows show the position of crystallite boundaries. B) High-resolution lattice-fringe image showing an extra brucite-like layer or extra talc-like layer (short fat arrow) developed in a well-ordered chlorite. The narrow arrow at the bottom marks the position of a crystallite boundary.

show a dramatic reduction in the degree of skewness and standard deviation. This reduction in asymmetry and spread presumably reflects the concentration of the small particles of authigenic illite in the clay fraction to the exclusion of the larger detrital components. Although the distributions of T_{δ} in the clay fraction also show reductions in skewness and standard deviation, as grade increases, the magnitude of these changes is significantly smaller than the changes in T_L .

Anchizonal and epizonal pelites do show significant differences in \bar{T}_L or \bar{T}_{δ} values between the size fractions (Table 1). Illite crystallites within the two clay fractions are 34 and 85% finer than those measured for the whole rock, and T_{δ} values are correspondingly 14 and 41% smaller. Although the standard deviation for the clay fractions are significantly reduced, no major changes in the skewness of the distributions occur, as was recorded in the diagenetic samples. The mean thicknesses and thickness distributions (T_L) of chlorite are very similar to those of illite, in both the whole-rock and clay frac-

tions (average differences in size of only 3% between N -weighted T_L values). As for illite, chlorite crystallites within the anchizonal and epizonal clay fractions are on average 36 and 76% finer than that measured for the whole rock, and \bar{T}_{δ} values are correspondingly 5 and 25% smaller. The standard deviation of crystallite thicknesses for chlorite in the clay fraction is also significantly reduced, and the skewness of these distributions is relatively low.

Log-transformed N -weighted T_L distributions for both illite and chlorite, presented in Figure 7 and 8, show slight asymmetry in the distributions, which are positively skewed. For illite, the degree of skewness generally decreases with increasing metamorphic grade, reflecting a tendency toward more lognormal shapes in the slates of anchizonal and epizonal grade. This decrease in skewness is not, however, recognizable in T_L distributions of chlorite. The shapes of T_L distributions for the whole-rock and clay-sized fractions show similarities, particularly for illite in SW2 and SW4, and

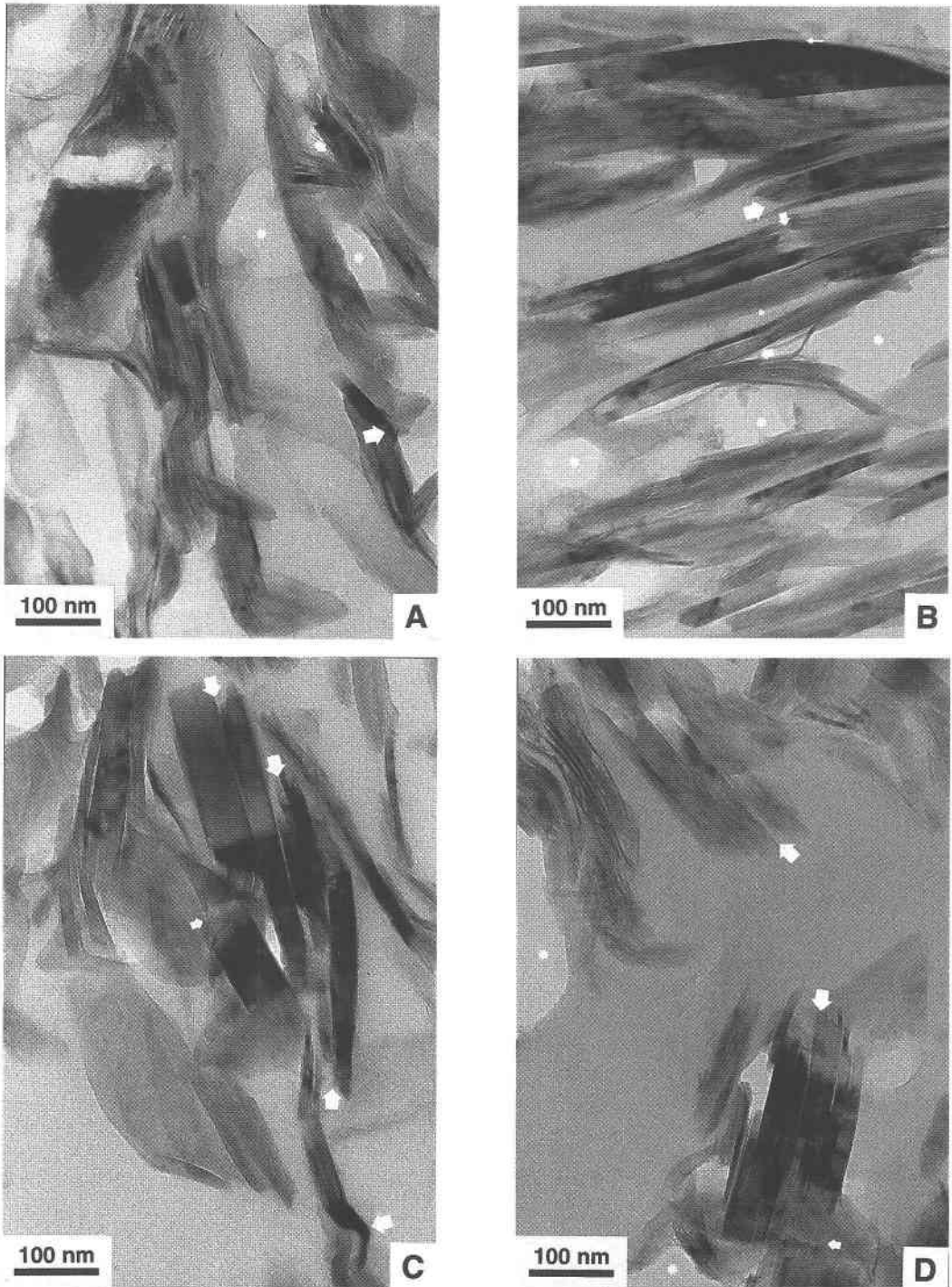


FIG. 6. TEM lattice-fringe images of clay separates for SW1, SW2, SW4 and SW6 (A – D). Damage incurred during ultramicrotoming is marked by the small fat arrows and with air-bubbles marked by stars. The larger fat arrows show damage attributed to initial crushing or ultrasonic disaggregation. The thin arrow in B) refers to a natural taper of a thicker crystallite of illite that forms the edge of a separate.

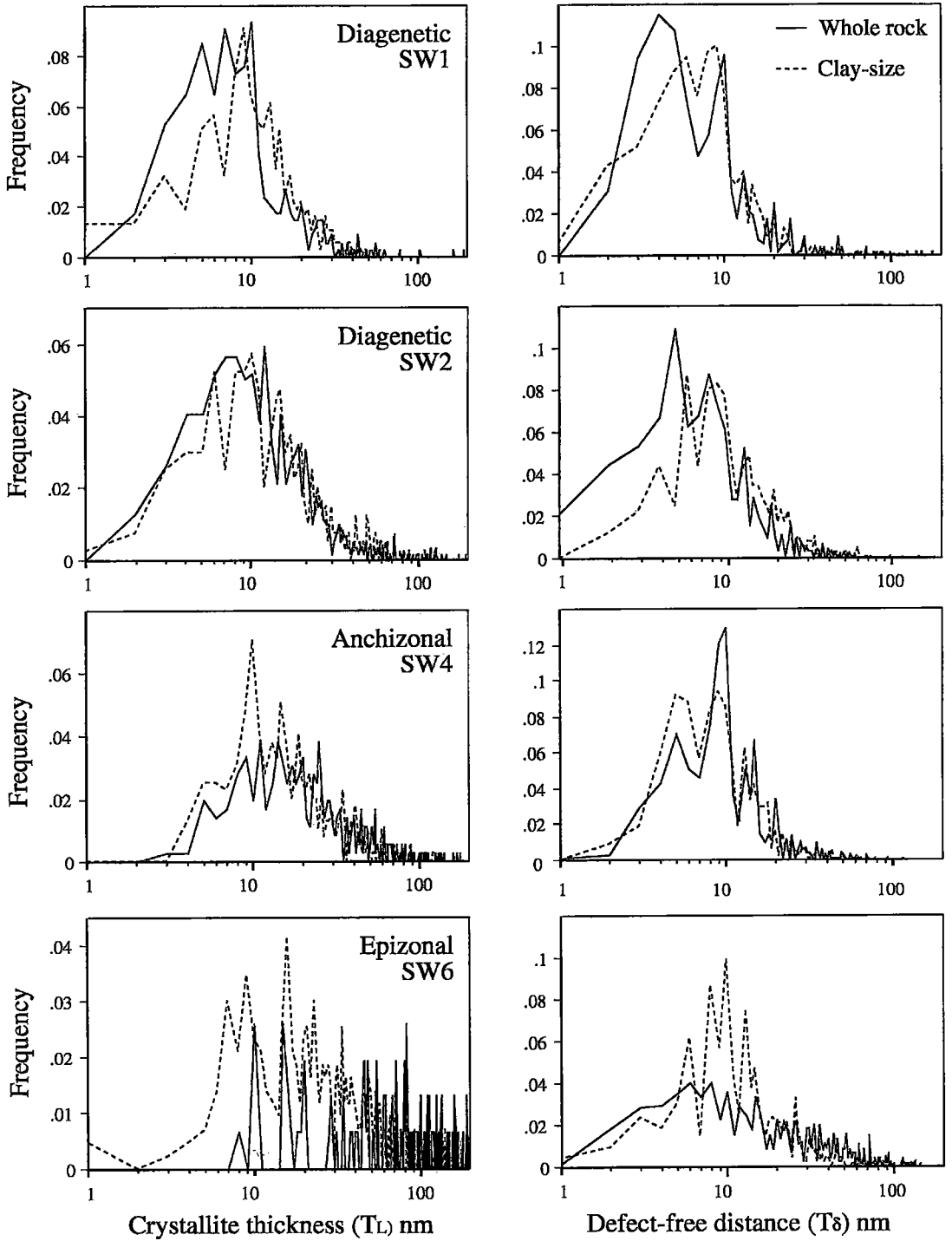


FIG. 7. N-weighted log-transformed distributions (T_L and T_S) for illite in whole-rock (drawn line) and clay-sized fractions (stippled) of the CIS pelitic samples.

TABLE 1. TEM-MEASURED N-WEIGHTED T_L AND T_S (nm) FOR ILLITE AND CHLORITE IN WHOLE-ROCK AND CLAY-SIZED FRACTIONS OF THE CIS SAMPLES

Zone CIS samples	diagenetic- SW1		diagenetic- SW2		anchi- SW4		epi- SW6	
	T_L	T_S	T_L	T_S	T_L	T_S	T_L	T_S
WHOLE ROCK								
Illite								
mean (N-weighted)	16	13	21	13	35	14	157	29
Skewness	10	7	9	4	4	3	2	2
Std. Dev.	36	21	34	12	37	12	156	26
n	342	522	622	950	363	745	154	750
α	2.3	2.1	2.6	2.3	2.6	2.4	4.6	3.0
β^2	0.7	0.7	0.7	0.5	0.5	0.4	1.0	0.9
CLAY FRACTION								
Illite								
mean (N-weighted)	14	10	20	14	23	12	38	17
Skewness	2	7	2	2	2	2	2	6
Std. Dev.	9	9	17	10	16	8	33	16
n	375	330	405	414	396	480	432	775
α	2.4	2.1	2.7	2.5	2.9	2.4	3.3	2.5
β^2	0.5	0.4	0.6	0.4	0.5	0.4	0.7	0.6
WHOLE ROCK								
Chlorite								
mean (N-weighted)	53	16	-	-	36	16	142	20
Skewness	2	3	-	-	9	3	2	6
Std. Dev.	63	13	-	-	60	16	141	55
n	45	187	-	-	174	239	81	407
α	3.5	2.6	-	-	3.2	1.4	4.2	2.2
β^2	1.2	0.4	-	-	0.5	0.1	1.1	1.0
CLAY FRACTION								
Chlorite								
mean (N-weighted)	20	11	-	-	23	12	34	19
Skewness	1	1	-	-	2	2	2	2
Std. Dev.	13	6	-	-	16	8	28	13
n	51	56	-	-	396	480	239	197
α	2.8	2.2	-	-	3.0	2.4	3.2	2.8
β^2	0.6	0.3	-	-	0.6	0.4	0.7	0.4

α and β^2 values are the shape parameters described by Eberl *et al.* (1998a).

chlorite in SW4. Clear differences in distributions between grain-size fractions are, however, notable for illite in SW1 and for both illite and chlorite in SW6. Log-transformed N-weighted T_S distributions for both illite and chlorite are more strongly skewed toward smaller sizes and show stronger deviations from lognormal curves than T_L distributions (Figs. 7, 8). T_S distributions are more positively skewed, reflecting the high abundance of small defects, and may be described as asymptotic in shape. The general similarity in the shapes of T_S distributions in whole-rock and clay-sized fractions suggests that the peaks and troughs in these distributions could be realistic, rather than artefacts of too few measurements.

Table 2 presents area-weighted and volume-weighted data for both illite and chlorite. In the diagenetic whole-rock samples, the area- and volume-weighted mean thicknesses show major increases related to the influence of larger crystallites, which may reach up to an order of magnitude larger in size than mean N-weighted values. With increasing metamorphic grade, the discrepancy between N-, area- and volume-weighted mean sizes decreases as the mean and maximum thicknesses become closer. The differences in the mean sizes are most significant in the whole-rock fractions owing to a greater portion of larger crystallites. In general, area-

TABLE 2. TEM-MEASURED AREA- AND VOLUME-WEIGHTED T_L AND T_S (nm) FOR ILLITE AND CHLORITE IN WHOLE-ROCK AND CLAY-SIZED FRACTIONS OF THE CIS SAMPLES

Zone CIS samples	diagenetic- SW1		diagenetic- SW2		anchi- SW4		epi- SW6	
	T_L	T_S	T_L	T_S	T_L	T_S	T_L	T_S
WHOLE ROCK								
Illite								
Area-weighted mean	56	25	102	33	61	17	186	29
Volume-weighted mean	294	89	153	47	112	30	344	52
CLAY FRACTION								
Illite								
Area-weighted mean	19	9	33	17	28	13	56	19
Volume-weighted mean	24	14	49	24	42	18	84	28
Area-weighted								
α	2.8	2.0	3.2	2.6	3.1	2.4	3.7	2.7
β^2	0.3	0.4	0.6	0.8	0.5	0.3	0.6	0.5
WHOLE ROCK								
Chlorite								
Area-weighted mean	82	15	-	-	85	20	170	21
Volume-weighted mean	139	25	-	-	336	41	260	194
CLAY FRACTION								
Chlorite								
Area-weighted mean	20	11	-	-	44	17	44	18
Volume-weighted mean	26	14	-	-	101	24	63	26

α and β^2 values are the shape parameters described by Eberl *et al.* (1998a).

and volume-weighted means are, on average, ~2 times and ~5 times larger than N-weighted means, respectively. Within clay fractions, corresponding differences are smaller, with the area- and volume-weighted means ~1 times and ~2 times larger. The shape parameters α and β^2 [the mean and variance of the natural logarithms of the sizes, as defined by Drits *et al.* (1998) and Eberl *et al.* (1998a)] for area-weighted thickness distributions of illite in the clay fraction are also presented for comparison with the N-weighted distributions given in Table 1. Whereas α values clearly increase, β^2 values generally decrease, reflecting larger mean thickness of crystallite and a reduction in variance when weighted by area.

Profile modeling using NEWMOD

In order to assess the extent to which crystallites and their lattice imperfections measured in TEM images acted as X-ray scattering domains, the area-weighted T_L , T_S and $T_L + T_S$ size distributions were used as input data (N) in the program NEWMOD (Reynolds 1985) to model reflections for comparison with naturally measured XRD profiles. Peak reflections were simulated for the three sets of size distributions, assuming that each selected group of thicknesses act as X-ray scattering domains. The results presented in Figure 9 show three sets of dashed curves representing the left side of scaled 002 NEWMOD profiles of illite. As expected, T_L distributions produce the narrowest peaks, and T_S distributions, assuming that all defect-free distances act as X-ray scattering domains, the broadest peaks. The $T_L + T_S$ curve, which treats all thicknesses measured as

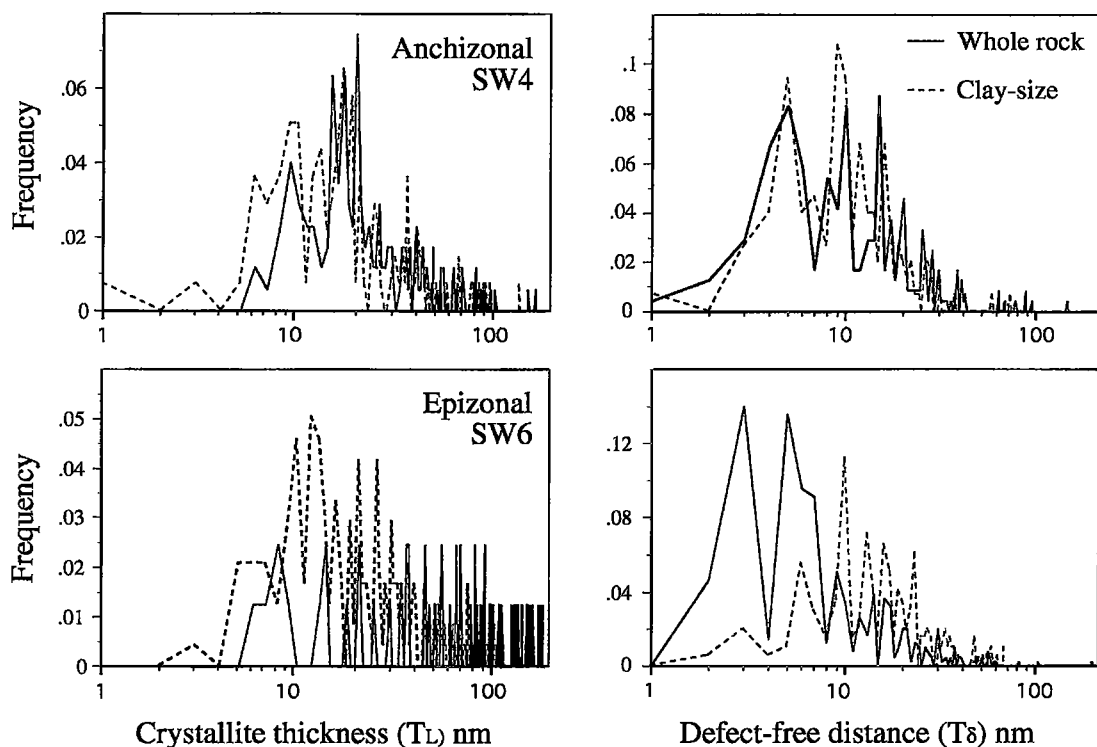


FIG. 8. N-weighted log-transformed distributions (T_L and T_δ) for chlorite in whole-rock and clay-sized fractions of standards SW4 and SW6.

scattering domains, produces intermediate curves lying between T_L and T_δ profiles. Measured XRD profiles of samples for the same 2θ range are also presented from which the PVP-silicon background, the $K\alpha_2$ component and the instrumental broadening were removed in order to allow direct comparison with the NEWMOD modeled profiles. In general, the measured XRD curves match the T_L profiles reasonably well, except for diagenetic sample SW2, which yields a curve that is significantly broader than that modeled from T_L data, suggesting that a significant number of T_δ made acted as X-ray scattering domains.

Thickness measurements by X-ray diffraction

Table 3 presents the results from three sets of diffraction profiles analyzed using MUDMASTER and a Siemens (1991) Single-line method (version 2.2). Set (1) consist of raw XRD data profiles, set (2) comprises XRD profiles that were first stripped of the PVP-silicon background and $K\alpha_2$ radiation using Siemens software prior to size analysis, and set (3) are the NEWMOD profiles calculated from the area-weighted TEM-measured T_L data (Table 2). Overall, there is a good corre-

spondence between the various XRD methods applied in this study and the TEM data. Mean thicknesses for dataset 2, calculated using the integral peak-width method of Drits *et al.* (1998), are plotted for illite and chlorite in Figure 10. This method produces results that are linearly related to the TEM-determined area-weighted T_L data, and the curve shows a 1:1 relationship, despite the fact that this method does not take into account instrumental broadening. The results of W-A analyses of the three sets of profiles also are presented in Table 3. NEWMOD-calculated patterns (set 3) were first run in order to verify the optimal input parameters for MUDMASTER [as tested by Drits *et al.* (1998) for broader clay-mineral peaks]. Both mean thickness and thickness distributions of crystallites in the TEM input data were satisfactorily reproduced (compare Table 2 with Table 3) using the shortened analytical ranges of 6.5 to $9.2^\circ 2\theta$ for illite 001, and 15 to $18^\circ 2\theta$ for illite 002 reflections, which successfully avoided adjacent reflections. All other settings were set at the recommended values.

Set (1) profiles were analyzed using the default options of Eberl *et al.* (1998b) for PVP-illite, which produced W-A mean thicknesses (\bar{T}_e) that are generally

TABLE 3. XRD-DETERMINED AREA-WEIGHTED MEAN CRYSTALLITE THICKNESSES AND STRAIN FOR ILLITE AND CHLORITE IN CLAY-SIZED FRACTIONS OF THE CIS SAMPLES

Zone CIS samples	diagenetic- SW1		diagenetic- SW2		anchi- SW4		epi- SW6	
	001	002	001	002	001	002	001	002
Illite								
(1) \bar{T}_l	18	20	20	17	24	22	50	35
(2) \bar{T}_l	19	21	22	18	26	24	56	39
(2) \bar{T}_s-1	20	17	21	21	26	22	62	53
(3) \bar{T}_l	18	17	36	31	32	27	-	52
(1) \bar{T}_e	10	6.5	12	7	16	10	26	15
α	2.4	2.2	2.5	2.2	2.7	2.6	3.0	2.8
β^2	0.6	0.7	0.5	0.7	0.4	0.9	0.5	0.8
Tc		11		14		18		28
RMS (σ) Å		0.24		0.24		0.21		0.16
(2) \bar{T}_e	16	13	17	14	21	19	37	31
α	2.8	2.9	2.8	2.8	2.9	3.2	3.2	3.3
β^2	0.6	0.8	0.4	0.6	0.3	0.6	0.4	0.4
Tc		15		18		22		32
RMS (σ) Å		0.17		0.18		0.11		0.08
(3) \bar{T}_e	19	18	34	31	29	27	-	44
α	2.8	2.8	3.3	3.3	3.1	3.1	-	3.9
β^2	0.3	0.3	0.4	0.5	0.4	0.3	-	0.4
Tc		20		35		29		29
RMS (σ) Å		0.07		0.04		0.05		0.05
Chlorite/kaolin*	002	003	002*	-	002	003	002	003
(1) \bar{T}_l	-	35	15	-	32	44	49	54
(2) \bar{T}_l	-	35	15	-	32	47	53	62
(2) \bar{T}_s-1	-	41	20	-	32	34	49	45

Calculations were made using MUDMASTER unless otherwise stated. The datasets: (1) Raw XRD data files of PVP-treated thin-film analyses. (2) XRD profiles stripped of the PVP-silicon background and $K\alpha_2$ radiation using Siemens software prior to size analysis. (3) NEWMOD-calculated diffraction patterns modeled from area-weighted TEM-measured \bar{T}_l data.

Abbreviations from Eberl *et al.* (1996, 1998b): \bar{T}_l : thicknesses measured by the integral peak-width method of Drits *et al.* (1998); \bar{T}_e : extrapolated thicknesses measured by the W-A method; α and β^2 values refer to the mean and variance of log-transformed data; Tc: extrapolated thicknesses by the W-A method for strain-corrected reflections; RMS(σ) Å: root mean square of strain.

Other symbols: \bar{T}_s-1 : thicknesses measured by the single-line method of Siemens WINCRYSIZE (1991, version 2.2).
The thicknesses are reported in nm.

half those of the TEM-measured data. The distribution of XRD-determined crystallite thicknesses also show no similarity with either \bar{T}_l or \bar{T}_s profiles measured by TEM. Strain is correspondingly high, with the root mean square of strain (RMS) ranging from 0.08 in the instrumental standard to 0.24 in the diagenetic samples. Set (2) profiles were analyzed using the same range of settings, but the peaks were treated exactly the same way as the NEWMOD-calculated patterns, with LpG² corrections for pyrophyllite edges. The results appear more realistic, with values on average 30% narrower than the TEM data, and smaller concentrations of strain were detected (RMS = 0.06–0.18). There is also a reasonable correspondence between the amount of strain detected by XRD and \bar{T}_s values measured by TEM. The option for correcting the effect of instrumental broadening in MUDMASTER, using the broadening profile of Mf1c, had no effect on measured thicknesses.

The best-matching combinations between XRD-determined thickness distributions and the TEM-measured

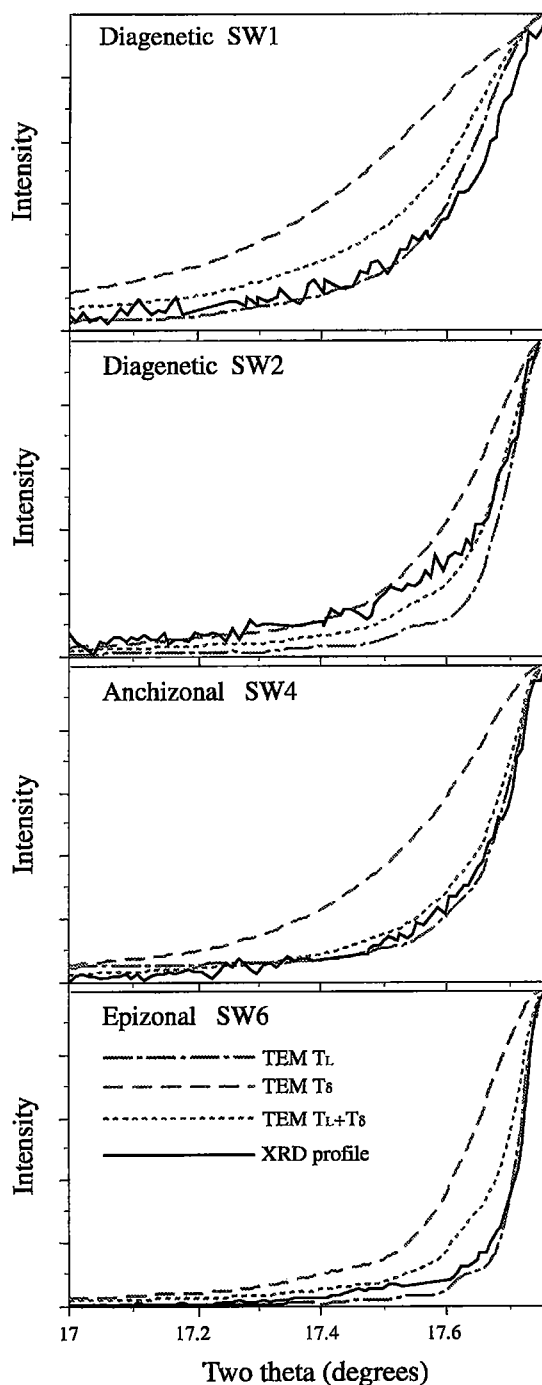


FIG. 9. Comparisons between NEWMOD-calculated patterns simulated for the 002 peak of illite at 5 Å ($17.75^\circ 2\theta$) using from area-weighted TEM measurements of thickness on separates and directly measured XRD profiles (SW1–SW6).

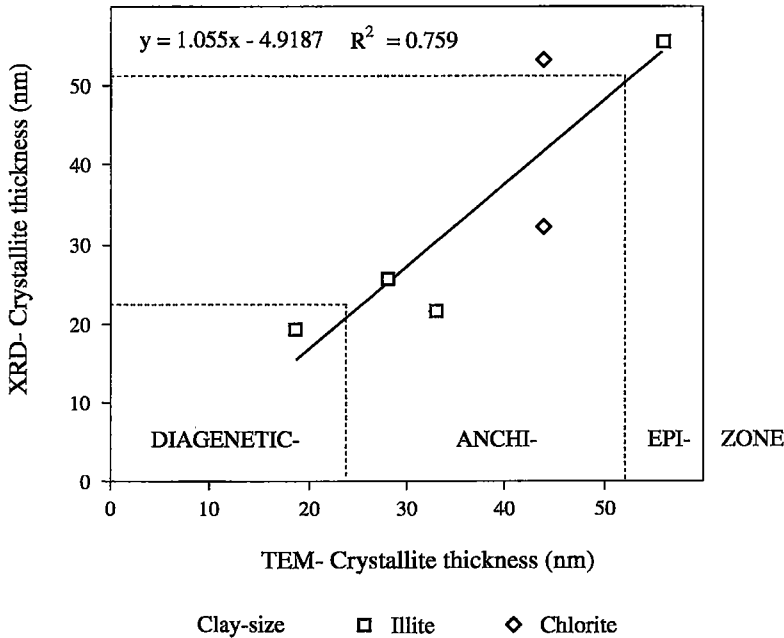


FIG. 10. Plot of the area-weighted mean thickness of crystallites for illite and chlorite determined by TEM and the XRD method of Drits *et al.* (1998) for clay-sized fractions of the CIS pelitic samples (data from Table 3, dataset 2).

thicknesses were produced from the illite 001 reflection of dataset (2), as shown in Figure 11. Although the log-transformed area-weighted thickness distributions of crystallites measured by XRD show asymmetrical, positively skewed profiles, the best match is still generally poor. Crystallites <8 nm across have not been measured owing to problems of accurately removing the background. Diagenetic pelite SW1 shows some similarity between the XRD- and TEM-determined distributions, with the peak maximum of the XRD-derived profile corresponding well with the peak maximum of the TEM distribution, and both slopes having similar gradients. The peaks in the large crystallite region of the XRD-derived profile may represent ripples in the Fourier calculation, or may be caused by the presence of large crystallites that are difficult to statistically measure by TEM, but have a large influence on the area-weighted XRD measured sizes. The thickness distribution of crystallites in diagenetic pelite SW2 do not show a good correspondence between the two curves. The peak maximum of the XRD profile lies at smaller sizes than the TEM profile; the XRD-determined distribution is strongly asymmetrical, whereas the TEM curve is more normal. The right-hand, larger-sized slopes of the distributions, however, match reasonably well, and ripples at large sizes occur in both profiles of SW2. Pelite SW4 from the anchizone shows a rough correspondence be-

tween the XRD and TEM data, but the distributions for the pelite SW6 from the epizone show little similarity. The latter is probably due to the insufficient number of counts used to define this TEM profile.

DISCUSSION

Deducing mechanisms of phyllosilicate growth and deformation in pelitic rocks from crystallite thickness and defect density

TEM observations of the CIS pelitic rocks reveal the full array of well-documented microstructures commonly recorded in prograde pelitic sequences spanning the transition from diagenesis (zeolite) to epizone (greenschist) grades of metamorphism. The characteristics of illite and chlorite in the diagenetic mudstones (SW1 and SW2), and the slates of anchizone (SW4) and epizone (SW6) grades show many features in common with those described in comparable rock types from the Welsh basin, U.K. (Merriman *et al.* 1990), the Subbetics of Spain (Nieto & Sánchez-Navas 1994), the Southern Uplands of Scotland (Merriman *et al.* 1995), the Bükkium of northeastern Hungary (Árkai *et al.* 1996) and the Gaspé Peninsula of Quebec (Jiang *et al.* 1997). Microstructural changes comprise an overall increase in the thickness of crystallites and a general decrease in

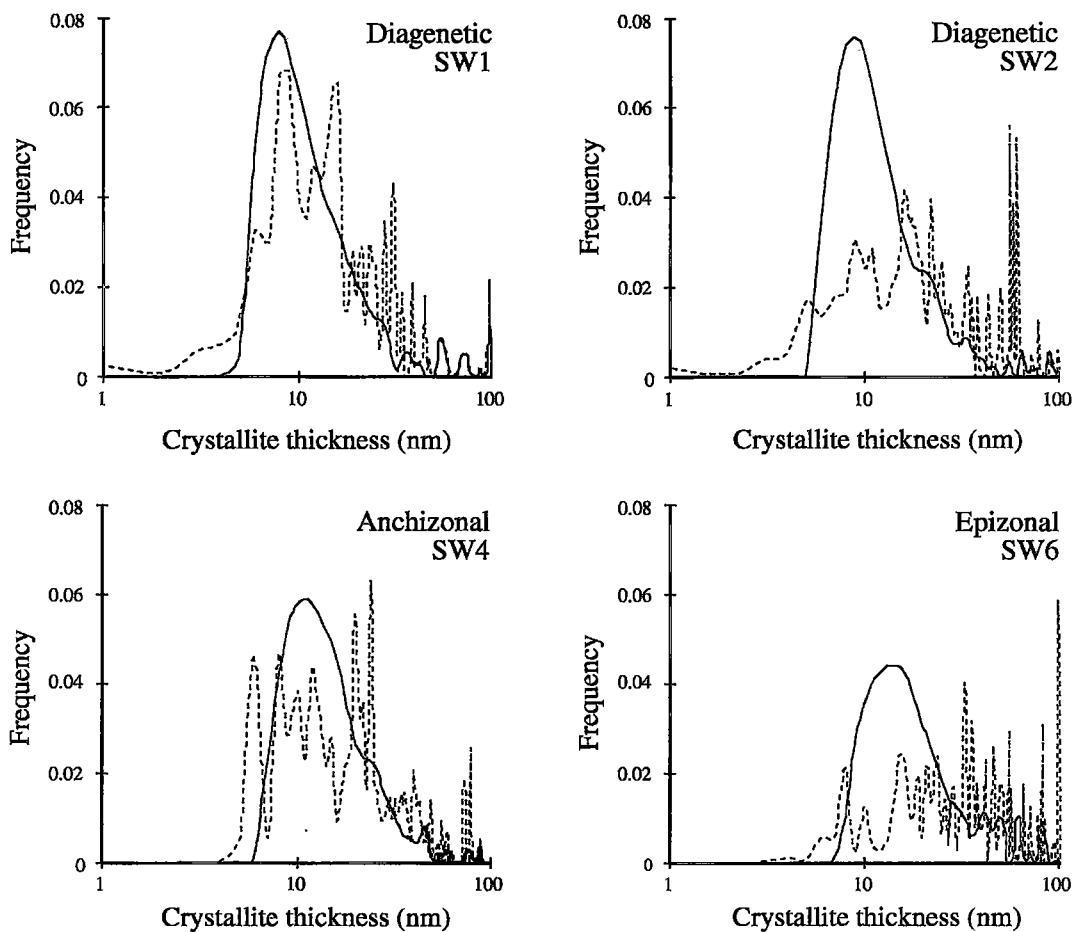


Fig. 11. Area-weighted thickness distributions of illite crystallites (SW1–SW6) determined by TEM (dashed line) and XRD (W–A method of MUDMASTER, solid line) for clay-sized fractions.

the concentration of defects with increasing metamorphic grade.

Despite the general similarities in microstructure, the thickness distributions of illite and chlorite crystallites in both whole-rock and clay-sized fractions are not ideally lognormal, as commonly described for many diagenetic clays and low-temperature metamorphic phyllosilicates (*e.g.*, Eberl *et al.* 1990, Dalla Torre *et al.* 1996, Merriman *et al.* 1995), but are generally slightly asymmetrical, with positive skewness toward small sizes. One approach to interpreting the meaning of these thickness distributions is to assume that all crystallite boundaries formed as growth surfaces, and the shape of each size distribution reflects a single population of phyllosilicate crystallites. Measured α and β^2 shape parameters (Table 1) and the modeling of Eberl *et al.* (1998a) can then be applied to deduce the mechanisms

of crystal growth. Adopting this procedure, the distributions of crystallite thickness yield α and β^2 values that lie between those expected for nucleation and growth, and for surface-controlled growth in open systems (Fig. 12). Such distributions could arise where phyllosilicates first form by continuous nucleation and growth, with β^2 increasing exponentially in relation to α (producing asymptotic curves), and then undergo a secondary supply-controlled growth, whereby α increases while β^2 remains constant (D.D. Eberl, pers. commun.).

Whereas there are indications that mineral growth occurred in an open system, with the formation of pressure-solution cleavages and abundant quartz–carbonate veins reflecting the mobility of diagenetic and metamorphic fluids, adoption of the approach of Eberl *et al.* (1998a) is questionable in the case of polydeformed pelitic rocks, such as those investigated in this study.

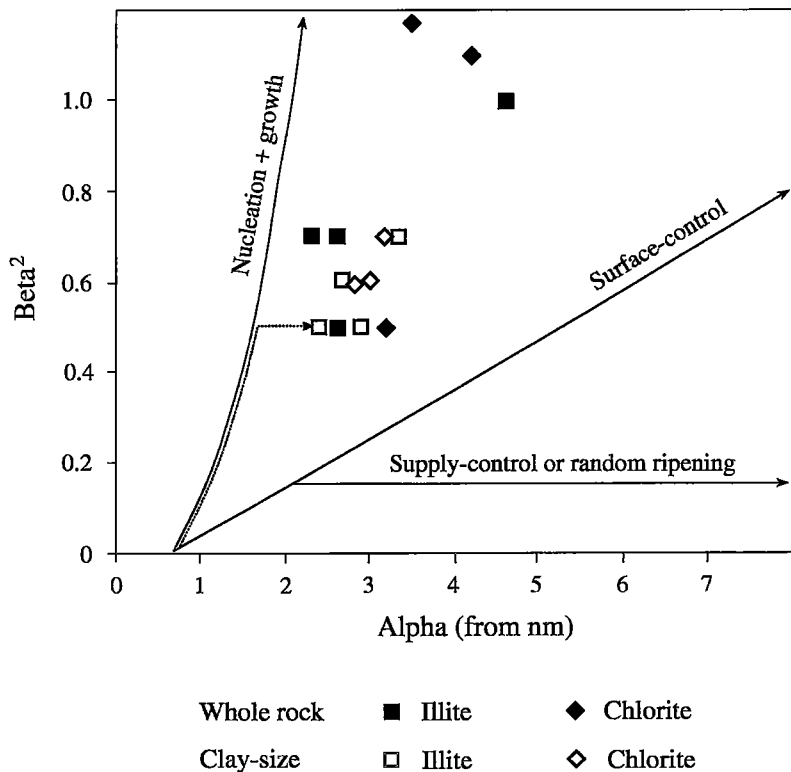


FIG. 12. α and β^2 shape parameters for crystallite thickness-distributions of the whole rock and clay-sized fractions of the CIS pelitic samples. The theoretical paths of particular growth-mechanisms are those calculated by Eberl *et al.* (1998a). The dotted line marks a possible path for the growth of diagenetic illite that first undergoes nucleation and growth, followed by a secondary stage of supply-controlled growth or random ripening.

Examination of phyllosilicate fabrics reveals that a greater number of complex stages of nucleation and growth took place than can be inferred from the shape of the thickness distributions. Two generations of authigenic illite can be recognized in diagenetic pelite SW1, which formed at different times in relation to the compaction of the sediment. Both generations are microstructurally heterogeneous, with small and defect-bearing crystallites stacked intimately together within larger aggregates (quasi-crystals). Further heterogeneity in this sample is also exemplified by the presence of large well-ordered illite-muscovite and chlorite grains of detrital origin, a portion of which may have been included in thickness measurements. Complex metamorphic fabrics are also present in the anchizonal and epizonal slates, which show that multiple generations of illite and chlorite formed at different times in relation to the main slaty cleavage. In both these samples, the principal mechanism that led to improved ordering of polytypes and the increase in crystallite thickness was

that of strain-induced solution and growth, accompanied by annealing and recrystallization. In the epizonal slate SW6, the replacement of defect-rich chlorite by less defect-rich illite-muscovite is the same mechanism of deformation and strain-induced growth as documented by Bons (1988).

Owing to the abundance of strain-related microstructures observed in the intact whole rock, a more favorable strategy for interpreting the shape of crystallite-thickness distributions in deformed pelites is that outlined by Merriman *et al.* (1995). They discussed the effects of strain rates on illite and chlorite in terms of modifications caused by subgrain formation, and processes of annealing and recrystallization. In such cases, crystallite thickness no longer provides a direct measure of the population of growth surfaces, but includes incoherency in the c^* direction caused by the formation and migration of subgrain boundaries (Merriman *et al.* 1995). Although the exact changes in the shape of illite and chlorite thickness-distributions that occur in response to

deformation are not well known, it is conceivable that subgrain formation produces strongly asymmetrical (asymptotic) thickness-distributions, skewed toward the smaller sizes (Ergun 1970), whereas crystallites controlled by annealing or recrystallization are expected to yield lognormal thickness-distributions, similar to those produced by the Ostwald ripening process (Cashman & Ferry 1988).

The microstructural characteristics described in this study are very much in accordance with such strain-related changes in crystallite thickness and defect density. Non-lognormal thickness-distributions of diagenetic crystallites of illite may reflect the abundance of subgrains formed during high strain-rates at lower temperatures, whereas the apparent tendency toward more lognormal shapes in anchizonal and epizonal slates probably represents annealing and recrystallization at higher temperatures. Similarly, the strongly asymmetrical, asymptotic-type profiles of the defect-free distances within crystallites, which represent a general measure of spacing between numerous types of lattice imperfections, yield distributions characteristic of those recorded in highly defect-ridden materials, such as diffusely scattering carbon (Ergun 1970). Many of these lattice imperfections probably formed during crystal-plastic strain under relatively high strain-rates, either during or after crystal growth.

Natural and damage-induced differences in crystallite thickness and defect density in clay separates

In order to concentrate the fine authigenic or metamorphic portion of a sample, and exclude larger grains not related to the same growth event, such as detrital material, the clay-sized fraction is routinely separated for XRD analysis. Clay separates commonly contain smaller crystallite-thicknesses than the matrix of the intact rock, and the shape of crystallite thickness-distributions are reduced in skewness and standard deviation (Jiang *et al.* 1997, Li *et al.* 1998). Despite these differences, the microstructural trends described for the whole-rock pelites are usually preserved in the separated clay-sized fraction. Whereas these characteristics could simply reflect natural grain-size-dependent differences in microstructure that accompany concentration of the smaller authigenic-metamorphic crystallites in the clay-sized fraction, Jiang *et al.* (1997) suggested that crystal damage inflicted during sample preparation may also be responsible for these changes. Such modifications, however, were envisaged to occur as a function of the inherent mineralogical and microstructural characteristics of the minerals. More specifically, Li *et al.* (1998) considered the improved lognormality of crystallite thickness-distributions recorded in their clay separates of Otago pelites as directly reflecting grinding damage incurred during sample disaggregation. They emphasized the dangers of interpreting growth mechanisms based on the study of disarticulated clay-sized separates.

Although masked by later damage caused by ultramicrotoming of the clay film, TEM observations of the CIS clay separates reveal that similar types of sample-preparation damage occurred by ultrasonic disaggregation, as that described by Jiang *et al.* (1997) and Li *et al.* (1998) in clay separates disaggregated by mechanical crushing. Modifications typically consist of splitting along natural boundaries of crystallites or intracrystalline defects, such as swelling layers and intragranular faults. Grain fragmentation running roughly parallel to the c^* direction caused by grain breakage and kinking also occurs, but this does not lead to direct changes in crystallite thickness. Although diagenetic samples contain more defects and heterogeneities, which can be split during disaggregation, such modifications are less common because the separated grains commonly comprise aggregates rather than individual crystallites. More damage is incurred as the grain size increases (in anchizonal and epizonal slates) where separates consist of individual crystallites or fragments of crystallites, which become concentrated in the clay-sized fraction. Clearly the impact of sample-preparation damage is significantly greater in rocks of higher metamorphic grade, and thus contributes to differences in mean thickness of crystallites between the whole rock and clay-sized fraction.

Despite the damage of crystals within clay separates, it is notable that the α and β^2 shape parameters for thickness distributions of both illite and chlorite crystallites plot along the same trend in α - β^2 space as that of the whole-rock data (Fig. 12). Interpretations of growth and deformation mechanisms deduced from the shape parameters of crystallite thickness-distributions therefore appear to apply equally to both grain-size fractions, indicating that damage occurred largely by crushing of the inherent microstructure of the minerals, as opposed to the initiation of new defects by grinding. In contrast to the opinion of Li *et al.* (1998), who suggest that extensive damage due to splitting will lead to the improved lognormality of thickness distributions, we consider that this type of damage is more likely to produce near-asymptotically shaped distributions, similar to those described for the defect-free distance measured for the CIS pelites. Whereas TEM observations do show that some of the originally optically parallel defect-structures in the intact rock may become split and transformed into crystallites, the extent of this process was not sufficient to significantly modify the α - β^2 trend shown.

Phyllosilicate microstructure and the broadening of X-ray-diffraction peaks

The term crystallite has been used in this study to represent a succession of optically parallel and uninterrupted lattice layers in the c^* direction of a given mineral phase, which in the case of metamorphic phyllosilicates may represent either crystal-growth surfaces or subgrain boundaries formed during

deformation. This definition is in accordance with that in the material sciences literature (e.g., Klug & Alexander 1974), whereby domain size and crystallite size are traditionally used interchangeably. A basic assumption of the XRD approach in the study of microstructure is that the size of X-ray-scattering domains provides a direct measure of the crystallite size (thickness), whereas lattice imperfections that cause small-scale variations in d values contribute to strain-type broadening of XRD profiles (Klug & Alexander 1974). In the case of phyllosilicates, there has been some divergence in opinion as to which microstructures observed in TEM lattice-fringe images act as X-ray scattering domains or contribute to strain-type broadening. Árkai *et al.* (1996) and Jiang *et al.* (1997) suggested that crystallites constitute the principal X-ray-scattering domains, whereas lattice imperfections such as layer terminations, dislocations, high-strain fields, and even swelling-layers, cause strain-broadening. In contrast, Dalla Torre *et al.* (1997) argued, on the basis of a TEM-XRD comparative study of white mica in metamorphic pelites from the Diablo Range (California), that many lattice imperfections such as dislocations, intergrown layers of smectite or incoherent layer-rotations, which cause variations in periodicity, also create X-ray-scattering domains. They equated the size of the X-ray-scattering domains to a defect-free distance in the c^* direction of white mica grains, rather than to crystallite thickness.

Our NEWMOD simulations of the broadening effects on crystallites and of defect-free distances measured by TEM provide greater support for the scenario of Árkai *et al.* (1996) and Jiang *et al.* (1997) than for that of Dalla Torre *et al.* (1997). The size of the X-ray-scattering domains corresponds in most cases to the crystallite thicknesses measured by TEM, with the exception of diagenetic illite in SW2. This sample contains larger mean thicknesses of crystallites than those measured by XRD, indicating that a portion of the defect-free distances acted as X-ray-scattering domains during diffraction. This, however, may simply reflect the difficulties in recognizing low-angle boundaries between crystallites in TEM images. Although the relationship between the defect-free distance and strain-broadening were not modeled in this study, there does appear to be a general but imprecise relationship between these features, as suggested by Árkai *et al.* (1996) and Jiang *et al.* (1997). This inference again implies that lattice imperfections within crystallites largely give rise to strain-broadening (distortion) involving variable lattice-spacing, as opposed to distinct incoherently diffracting X-ray-scattering domains.

Measurements of crystallite thicknesses by the XRD approach

Many of the limitations presented in earlier studies (Merriman *et al.* 1990, 1995, Nieto & Sánchez-Navas

1994, Árkai *et al.* 1996), which compared results between TEM and XRD methods without selecting the same grain-size fractions, or making the necessary weighting adjustments to the TEM-derived size data, have been overcome in this study. Assuming the area-weighted TEM-measured thicknesses of crystallites to be accurate, some of the available XRD methods applied in previous work (Warr & Rice 1994), and the refined methods tested in this contribution, can be directly compared and ranked in terms of their performance (Table 4). The integral peak-width method of Drits *et al.* (1998) and the Siemens single-line method successfully applied by Warr (1996) on New Zealand pelites of known mineral facies, gave good results and produced near 1:1 relationships for both illite and chlorite. The empirical results of Warr & Rice (1994), based on the Scherrer equation and a Siemens Warren-Averbach method (version 1.0), were indeed reasonable estimates of the crystallite thickness of the standards, with a mean difference of between 21–22%, despite suggested errors in this version of the WINCRYSIZE program (S. Krumm, pers. commun.). However, the W-A method of MUDMASTER, which works effectively to calculate mean thickness and thickness distributions of crystallites from NEWMOD-calculated patterns, did not produce results that matched well the thickness distributions of crystallites measured by the TEM approach. Mean sizes were at best over 30% smaller than TEM-based measurements, even when the PVP-background and $K\alpha_2$ radiation effects were removed prior to size analysis. It has been proposed that this discrepancy reflects the inadequacy of the TEM approach in measuring the smaller crystallites (D.D. Eberl, pers. commun.). However, the good correspondence between NEWMOD-calculated patterns simulated from the TEM data and the natural XRD profiles does not support this argument. We suggest that the size differences are more likely to reflect problems in accurately removing the background and instrumental broadening effects from

TABLE 4. COMPARISON OF AREA-WEIGHTED MEAN CRYSTALLITE THICKNESSES DETERMINED BY VARIOUS XRD METHODS

CIS samples	SW1	SW2	SW4	SW6	TEM A XRD (%)
TEM (\bar{t}_i)	19	33	28	56	-
Integral peak width method* (Drits <i>et al.</i> 1998)	19	22	26	56	10
Siemens Single-line (Siemens WINCRYSIZE, v. 2.2)	20	21	26	62	15
Scherrer equation (by peak width) Warr & Rice (1994)	14	20	26	50	21
W-A method (illite 002-005 pair) (Siemens WINCRYSIZE, v. 1.0)	13	18	27	52	22
W-A method Eberl <i>et al.</i> (1996)	16	17	21	37	31

*Denotes thicknesses for the CIS scale which best match the TEM constraints.

narrow XRD reflections. Owing to continuing uncertainties in applying the W–A method to metamorphic pelites, we recommend that the mean data on thickness of crystallites determined by the method of Drits *et al.* (1998) be adopted for the Crystallinity-Index Standard scale, as these values match well the TEM data. Despite this small refinement in the recommended mean thicknesses of crystallites (area-weighted), the size limits from the anchizone remain unchanged at 23 and 52 nm, respectively.

CONCLUSIONS

1. The crystallinity-index standards display the full array of typical microstructural changes documented in prograde pelitic sequences, with increases in crystallite thickness and a decrease in defect density. Log-transformed distributions of crystallite thickness are not typically normal, but slightly positively skewed. These distributions reflect complex histories of nucleation and growth, as well as structural modifications either by subgrain formation or annealing and recrystallization. Defect-free distances within crystallites yield asymptotic distributions reflecting the abundance of strain-induced microstructures.

2. Whereas disaggregation damage within the clay-sized fraction contributes to the reduction of crystallite thickness, particularly in the case of the anchizone and epizone slates, the similarities in α – β^2 trends for both grain-size fractions show that modifications have not changed the interpretation of crystal growth and deformation mechanisms deduced from the shapes of thickness distributions.

3. NEWMOD-calculated patterns using TEM constraints produced model profiles that confirm the direct correspondence of size of X-ray-scattering domains and crystallite thicknesses, as long as the data are weighted accordingly. Lattice imperfections such as layer terminations, optically planar defects with incoherent layer-rotations, and high-strain fields, constitute the main source of strain-broadening.

4. The integral peak-width method of Drits *et al.* (1998) produced mean thicknesses of crystallites directly comparable with TEM-measured data, whereas the W–A method of Eberl *et al.* (1996) did not calculate comparable thickness-distributions of crystallites. This disagreement probably reflects inadequate treatment of both background and instrumental broadening effects when dealing with narrow reflections from phyllosilicates.

ACKNOWLEDGEMENTS

D.D. Eberl is thanked for his help concerning sample preparation, and calculations using MUDMASTER. L.N. Warr acknowledges financial support from the DFG (project Wa 803/3–2), and F. Nieto, from the Spanish Ministry of Education and Research Group RNM–

0179 of the Junta de Andalucía (project nº PB96–1383). The authors also thank H. Kisch and K. Livi for their constructive reviews of this work.

REFERENCES

- AHN, JUNG-HO & PEACOR, D.R. (1986): Transmission and analytical electron microscopy of the smectite to illite transition. *Clays Clay Minerals* **34**, 165–179.
- _____ & _____ (1989): Illite/smectite from Gulf coast shales: a reappraisal of transmission electron microscope images. *Clays Clay Minerals* **37**, 542–546.
- ÁRKAI, P., MERRIMAN, R.J., ROBERTS, B., PEACOR, D.R. & TÓTH, M. (1996): Crystallinity, crystal size and lattice strain of illite–muscovite and chlorite: comparison of XRD and TEM data for diagenetic to epizone pelites. *Eur. J. Mineral.* **8**, 1119–1137.
- BANFIELD, J.F., BAILEY, S.W. & BARKER, W. (1994): Polysomatism, polytypism, defect microstructures, and reaction mechanisms in regularly and randomly interstratified serpentinite and chlorite. *Contrib. Mineral. Petrol.* **117**, 137–150.
- BONS, A.-J. (1988): Intracrystalline deformation and slaty cleavage development in very low-grade slates from the central Pyrenees. *Geologica Ultraiectina* **56**, 1–173.
- _____ & SCHRYVERS, D. (1989): High-resolution electron microscopy of stacking irregularities in chlorites from the central Pyrenees. *Am. Mineral.* **74**, 1113–1123.
- CASHMAN, K.V. & FERRY, J.M. (1988): Crystal size distributions (CSD) in rocks and the kinetics and dynamics of crystallization. 3. Metamorphic crystallization. *Contrib. Mineral. Petrol.* **99**, 401–415.
- DALLA TORRE, M., LIVI, K.J.T., VEBLEN, D.R. & FREY, M. (1996): White K-mica evolution from phengite to muscovite in shales and shale matrix melange, Diablo Range, California. *Contrib. Mineral. Petrol.* **123**, 390–405.
- DRITS, V.A., EBERL, D.D. & ŚRODOŃ, J. (1998): XRD measurement of mean thickness, thickness distribution and strain for illite and illite–smectite crystallites by the Bertaut–Warren–Averbach technique. *Clays Clay Minerals* **46**, 38–50.
- EBERL, D.D., DRITS, V.A. & ŚRODOŃ, J. (1998a): Deducing growth mechanisms for minerals from the shapes of crystal size distributions. *Am. J. Sci.* **298**, 499–533.
- _____, NÜESCH, R., SUCHA, V. & TSPURSKY, S. (1998b): Measurement of fundamental illite particle thicknesses by X-ray diffraction using PVP-10 intercalation. *Clays Clay Minerals* **46**, 89–97.
- _____, ŚRODOŃ, J., KRÁLIK, M., TAYLOR, B.E. & PETERMAN, Z.E. (1990): Ostwald ripening of clays and metamorphic minerals. *Science* **248**, 474–477.

- _____, _____ & NÜESCH, R. (1996): MUDMASTER: a program for calculating crystallite size distributions and strain from the shapes of X-ray diffraction peaks. *U.S. Geol. Surv., Open File Rep.* **96-171**.
- ERGUN, S. (1970): X-ray scattering by very defective lattices. *Phys. Rev.* **B 1**, 3371-3380.
- JIANG, WEI-TEH, PEACOR, D.R., ÁRKAI, P., TÓTH, M. & KIM, JIN-WOOK (1997): TEM and XRD determination of crystal size and lattice strain as a function of illite crystallinity in pelitic rocks. *J. Metamorphic Geol.* **15**, 267-281.
- KLUG, H.P. & ALEXANDER, L.E. (1974): *X-ray Diffraction Procedures* (2nd ed.). John Wiley & Sons, New York, N.Y.
- LANSON, B. & KÜBLER, B. (1994): Experimental determination of coherent scattering domain size distribution of natural mica-like phases with the Warren-Averbach technique. *Clays Clay Minerals* **42**, 489-494.
- LEE, JUNG HOO, AHN, JUNG-HO & PEACOR, D.R. (1985): Textures in layered silicates: progressive changes through diagenesis and low-temperature metamorphism. *J. Sediment. Petrol.* **55**, 532-540.
- LI, GEJING, PEACOR, D.R., BUSECK, P.R. & ÁRKAI, P. (1998): Modification of illite-muscovite crystallite-size distributions by sample preparation for powder XRD analysis. *Can. Mineral.* **36**, 1435-1451.
- LIVI, K.J., VEBLEN, D.R., FERRY, J.M. & FREY, M. (1997): Evolution of 2:1 layered silicates in low-grade metamorphosed Liassic shales of central Switzerland. *J. Metamorphic Geol.* **15**, 232-344.
- MERRIMAN, R.J., ROBERTS, B. & PEACOR, D.R. (1990): A transmission electron microscope study of white mica crystallite size distribution in a mudstone to slate transitional sequence, North Wales, UK. *Contrib. Mineral. Petrol.* **106**, 27-40.
- _____, _____ & HIRONS, S.R. (1995): Strain-related differences in the crystal growth of white mica and chlorite: a TEM and XRD study of the development of metapelitic microfabrics in the Southern Uplands thrust terrane, Scotland. *J. Metamorphic Geol.* **13**, 559-576.
- NIETO, F. & SÁNCHEZ-NAVAS, A. (1994): A comparative XRD and TEM study of the physical meaning of the white mica "crystallinity" index. *Eur. J. Mineral.* **6**, 611-621.
- PEACOR, D.R. (1992): Diagenesis and low-grade metamorphism of shales and slates. In *Minerals and Reactions at the Atomic Scale: Transmission Electron Microscopy* (P.R. Buseck, ed.). *Rev. Mineral.* **27**, 335-380.
- REYNOLDS, R.C., JR. (1985): *NEWMOD, a Computer Program for the Calculation of One-Dimensional Diffraction Patterns of Mixed-Layered Clays*. R.C. Reynolds, Jr., 8 Brook Dr., Hanover, New Hampshire.
- SIEMENS WINCRYSIZE (1991): *Crystallite Size and Microstrain* (versions 1.0 - 2.2). *Sigma-C GmbH*.
- ŚRODOŃ, J., ANDREOLI, C., ELSASS, F. & ROBERT, M. (1990): Direct high-resolution transmission electron microscopic measurement of expandability of mixed-layer illite/smectite in bentonite rock. *Clays Clay Minerals* **38**, 373-379.
- _____, & ELSASS, F. (1994): Effect of the shape of fundamental particles on XRD characteristics of illitic minerals. *Eur. J. Mineral.* **6**, 113-122.
- VEBLEN, D.R., GUTHRIE, G.D., LIVI, K.J.T. & REYNOLDS, R.C., JR. (1990): High resolution transmission electron microscopy and electron diffraction of mixed-layer illite/smectite: experimental results. *Clays Clay Minerals* **38**, 1-13.
- WARR, L.N. (1996): Standardized clay mineral crystallinity data from the very low-grade metamorphic facies rocks of southern New Zealand. *Eur. J. Mineral.* **8**, 115-127.
- _____, PRIMMER, T.J. & ROBINSON, D. (1991): Variscan very low-grade metamorphism in southwest England: a diastathermal and thrust-related origin. *J. Metamorphic Geol.* **9**, 751-764.
- _____, & RICE, A.H.N. (1994): Interlaboratory standardization and calibration of clay mineral crystallinity and crystallite size data. *J. Metamorphic Geol.* **12**, 141-152.

Received December 3, 1997, revised manuscript accepted December 22, 1998.